Estimation of thin fracture aperture in a marble block by GPR sounding

L. SAMBUELLI and C. CALZONI

DITAG, Politecnico di Torino, Italy

ABSTRACT   In order to optimize the cutting of the marble blocks to be used in the restoration of the dome of the Holy Shroud Chapel of Turin cathedral, some GPR tests have been done in a laboratory to detect thin fractures in a marble block. We made some preliminary measurements to estimate the GPR wave velocity in an intact block and to calculate the permittivity of the marble. Then, the block was cut and GPR measurements with different fracture fillings and fracture apertures were performed. The results demonstrate that with at 2 GHz in antenna a fracture, a millimeter open, can be detected. An analysis carried out on the experimental reflection coefficients with the thin layer theory, allowed us to estimate the different fracture apertures. We found the possibility of estimating fracture apertures ranging from 1/10 to 1/5 of the wavelength at 2 GHz in air. The phase and the amplitude of the reflected signals with different fillings demonstrated the possibility of detecting thin fractures and discriminating between dry- or water -saturated fillings.

1. Introduction

In the night between the 11th and the 12th of April 1997 a fire seriously damaged the Holy Shroud Chapel of Turin Cathedral. At present, almost all the marble blocks covering the inner surface of the Chapel dome have a fracture system sub-parallel to the exposed faces. Some of the blocks can be restored, others are irreparably damaged and have to be substituted. To this purpose, the ancient quarries of "Bigio di Frabosa" marble, which historically provided the material used to build the chapel, will be re-opened. Smaller sub-blocks of sizes suitable to replace the ones in the dome will be cut from the quarry blocks. The sub-blocks will be reproduced with the shape and the mouldings made by numerically controlled machines. This process is expensive and the detection of fractures in quarry blocks would be useful to avoid the moulding of cracked sub-blocks and to optimize the resizing of sub-blocks.

A technique able to detect and locate nearly-closed fractures in marble blocks in the quarry yard, before their resizing and their submission to the moulding profiling, was required. Besides the detection and the localization, the possibility of estimating the fracture aperture has also been investigated.

The time-schedule for the restoration works will need a fast and highly resolutive survey method, therefore we focused our attention on the GPR. Actually, fractures filled with air within the blocks would prevent any acoustic signals to investigate beyond the fracture itself, unless a time-spending tomographic procedure is set up. On the other hand, a GPR signal would easily detect and go through the fractures filled with air and allow the investigation of the remaining

volume of the block. We then proposed a high frequency GPR survey, in near-zero offset reflection mode, with double-polarized antennas along parallel lines over at least two orthogonal faces of the block.

The detection of fractures and thin layers in various materials with GPR is a well known investigation field. The GPR has already been applied successfully to fracture detection in various types of rocks: granite (Myeong-Jong *et al.*, 2004; Porsani *et al.*, 2006), gneiss (Grasmueck, 1996), limestone (Grégoire *et al.*, 2003; Apel and Dezelic, 2005), dolomite (Tsoflias *et al.*, 2004), marble (Grandjean and Gourry, 1996; Ferrero *et al.*, 2007) and dry salts (Annan *et al.*, 1988).

In the present case, since the quarry still has to be re-opened, we worked in a laboratory on a block of "Bigio di Frabosa" marble. We began the investigations with the block intact in order to estimate the propagation velocity and to check if some anomalous concentration of calcite in the block reflected the GPR signal. Then, we cut the block and tested the reflection of the artificial air-filled fractures at different apertures. Later, we acquired the radar traces with different fillings in the fracture: first, we inserted an aluminum foil, then dry marble cuttings, a water film and finally, a thin layer of saturated marble cuttings.

2. Measurements of the intact block

The size of the intact block was 0.85 m × 0.70 m × 0.39 m. We acquired all the GPR measurements with a K2 IDS system and an Aladdin antenna which contains two orthogonal 2 GHz dipoles in its box: one longitudinal and the other orthogonal to the profile direction; in this way, we could appreciate the polarization effect. We acquired profiles both in the X and Y direction, according to the scheme in Fig.1.

We acquired one trace every 2 mm, the recording window was 20 ns with a sampling interval of about 0.02 ns. Neither filters nor gains were applied during acquisition. Knowing the dimension of the block and picking the reflection times of the block bottom, we estimate the velocity V in 0.097±0.0005 m/ns and a range of the relative permittivity ε_m from 9.46 to 9.66.

We processed the data with the Sandmeier Reflex Win$^{©}$ software, using the following steps: move start time, time cut, dewow, Kirchoff migration and Butterworth bandpass filtering (500-2800 MHz). In Fig. 2, the raw (a) and the processed (b) data referred to the central profile along the Y direction, with transversal dipole are shown. It is clear that no reflection occurs within the block
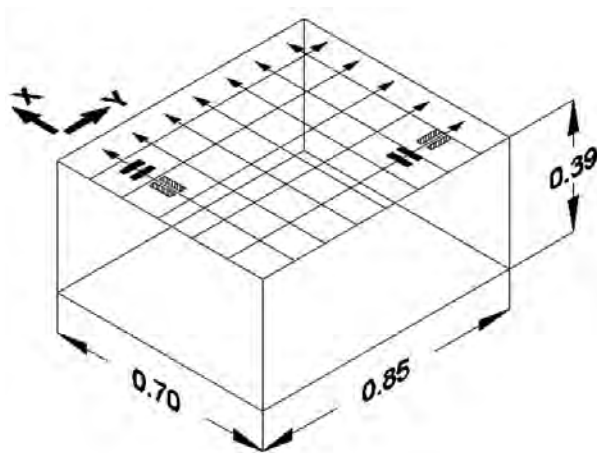

Fig. 1 - Measurement acquisition scheme on the intact block.
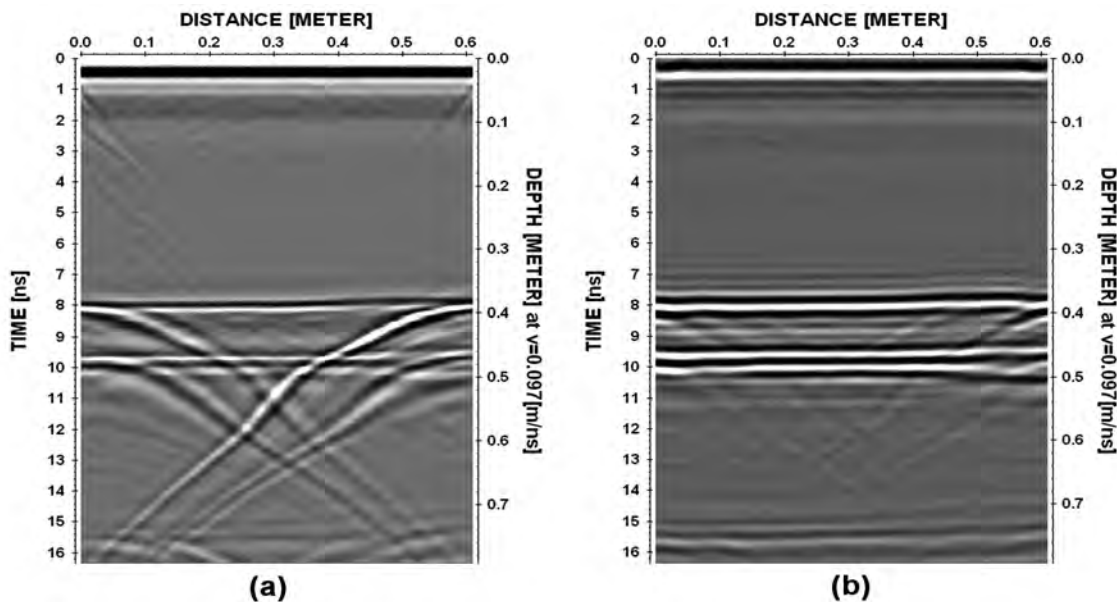
Fig. 2 - Comparison between the raw (a) and the processed (b) radargrams acquired on the intact block (central profile along the Y direction, transversal dipole).

even in correspondence to a clearer band in the marble related to a highest content of calcite.

3. Measurements of the cut block

To verify the GPR capability of localizing joints, we made an artificial fracture cutting the block as shown in Fig. 3.

Other similar experiments are referred to in literature with the aim of studying both the GPR resolution (Dezelic, 2004) and the possibility of estimating the electromagnetic properties of the fracture filling materials (Grégoire and Hollender, 2004).

For reasons inherent to this paper's organization, we now illustrate the results obtained from the tests performed on the cut block with different fillings, even if they were done after the ones with different fracture apertures.
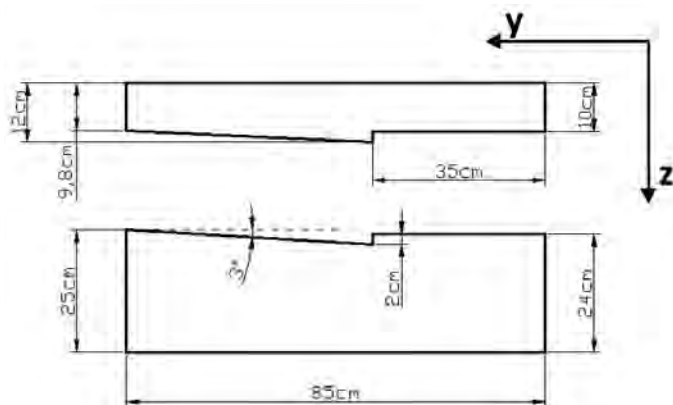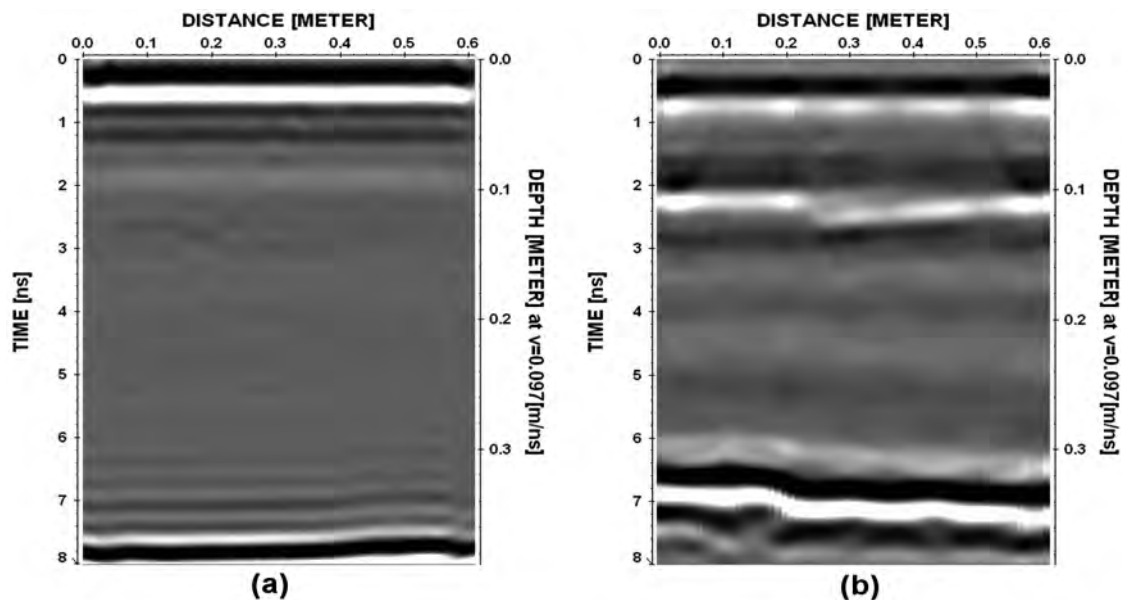

Fig. 3 - Scheme of the cut block.

Fig. 4 - Radargrams corresponding to the measurement along the central Y profile: (a) on the intact block, and (b) on the block after the cut (with the edge of the fracture in contact).

3.1. Measurements of the cut block with different fillings

According to the modeling results, we made the cut at 10 cm from the acquisition plane which is roughly 2 wavelengths at 2 GHz in marble.

We performed an acquisition with the empty fracture and the two edges closed. The acquisition parameters and the processing steps were the same as those used for the intact block, but we collected only the Y profiles with transverse and parallel dipoles. In such a configuration, we had the dipoles parallel (Ex) and orthogonal (Ey) to the fracture step. The resulting Ex radargram of the central Y profile is shown in Fig. 4b where, for comparison purposes, the Ex radargram of the intact block is also shown (Fig. 4a). The fracture is clearly visible even if its aperture was about 1/150 of the wavelength in air (the filling material) and the relative permittivity ratio marble/air was 9.5/1.

Then, we filled the fracture with 4 different materials: first with an aluminum foil, which provided also a reference reflected signal, after with dry cuttings from the stone dust, successively with a water film and finally with saturated cuttings. A part from the aluminum foil, the other materials were chosen to simulate the fillings that could be found in real quarry conditions. For each experiment, we used the same acquisition scheme adopted in the test with the edges of the fracture closed. The acquisition parameters and the processing steps were equal to the ones adopted for the intact block measurements. All the experiments demonstrated that the fracture is easily identifiable by GPR. In Fig. 5, the radargrams obtained with the fracture closed and the different fillings are shown. Only the one referred to the water film does not show a clear reflection in reproducing the fracture shape. This is due to the fact that water was poured on the lower part of the block, thus leaving some surfaces of the upper face of the fracture dry. Moreover,
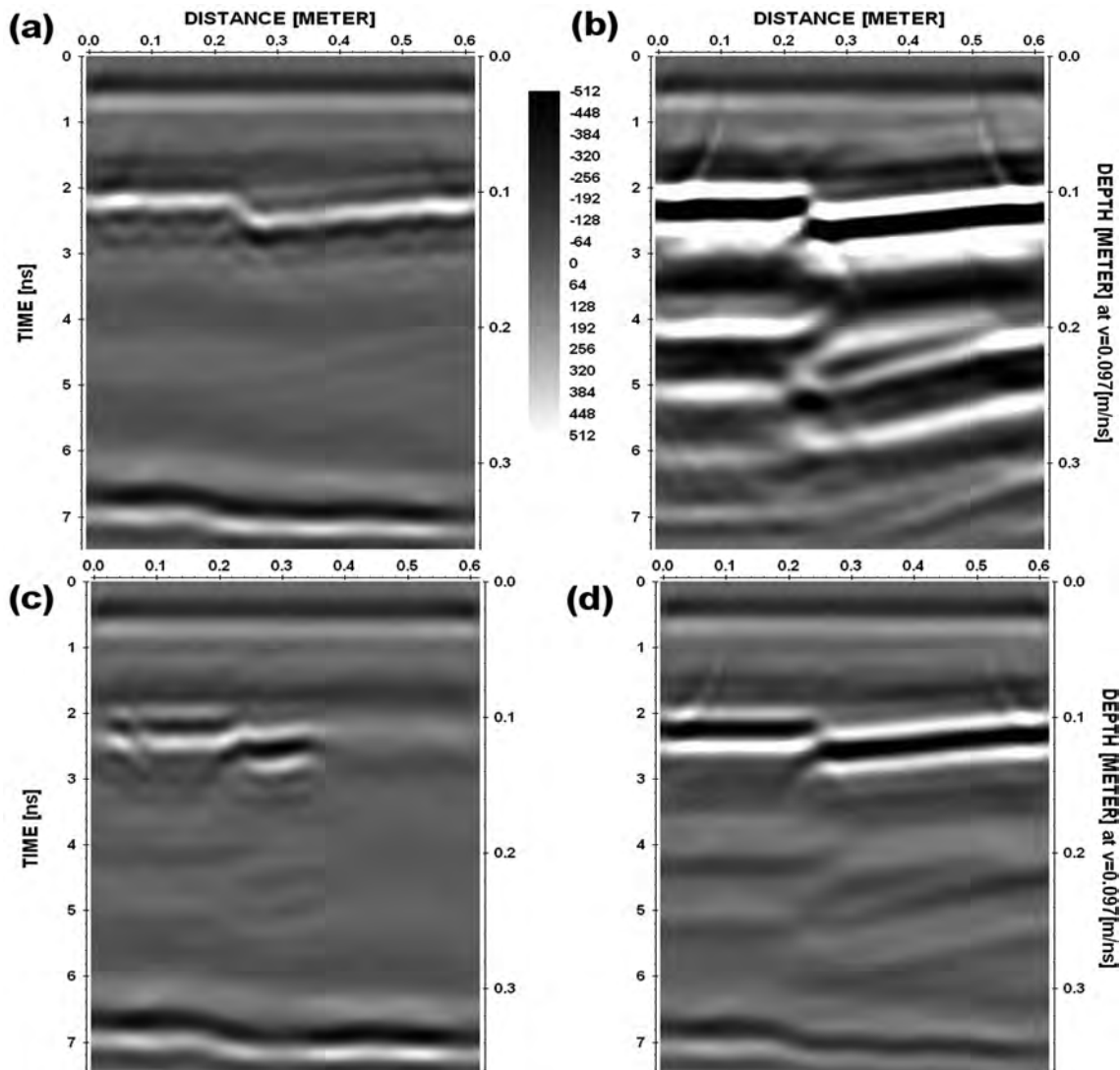
Fig. 5 - Radargrams obtained with different fillings: (a) dry cuttings; (b) aluminum foil; (c) water film; (d) saturated cuttings.

the water percolated toward the lower part of the step thus producing a highly reflective pond. The inversion of the polarity is also clear when the fillings are aluminum or saturated cuttings (Figs. 5b and 5d), instead of dry cuttings (Fig. 5a). Figs. 5b shows that according to the theory the aluminum foil gives the highest reflectivity. This is put in evidence by the high amplitude of reflections, by the strong multiples and by the fact that the bottom of the block is invisible. The electromagnetic field oscillates between the surface and the aluminum foil. Figs. 5a and 5d show that the reflectivity of the saturated cutting is higher than the one of the dry cuttings. This is put in evidence by the higher amplitude of reflection and by the stronger multiples below the fracture filled with saturated cuttings.
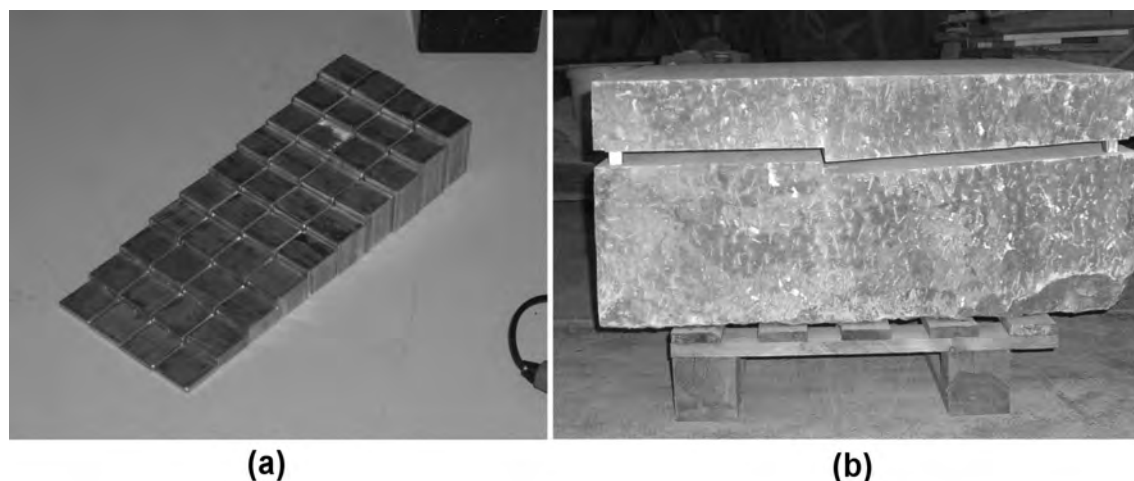
Fig. 6 - Pads used to change the fracture aperture (a), block with the fracture opened with pads (b).

3.2. Measurements of the cut block with different apertures

We then tried to estimate the fracture aperture. A thin layer thickness estimation with GPR is an exploited field of research. For instance, Riek *et al.* (1990) and Koh (1997) worked on thin ice layers. Some authors worked on fractures in rocks or thin sedimentary layers (Hollender and Tillard, 1998; O'Neill, 2000; Guha, 2004; Talley *et al.*, 2005) while others studied the problem in pavements (Yamamoto *et al.*, 2004; Al-Qadi and Lahouar, 2005; Lahouar and Al-Qadi, 2008).

With a set of pads (Fig. 6a), placed at the four corners of the fracture surface (Fig. 6b), we increased the aperture from 0 to 30 mm, in 3 mm steps.

The traces at Y=10 cm (central profile, Y direction, Ex) obtained with different apertures and fillings are shown in Fig. 7. Comparison of the traces does not highlight any distinct reflection coming from the upper and the lower edge of the fracture. Inversion of polarity appears clearly when the fillings are aluminum or water or saturated cuttings as in Fig. 7. On the other hand, an increase in the reflection amplitude is evident when the fracture aperture increases.

We then analyzed the amplitude of the reflected signals. The upper part of the cut block, where the GPR pulse travelled before being reflected by the fracture upper edge, was the same for all the experiments. Then, we could obtain the reflection coefficient related to each fracture aperture by normalizing the maximum reflected amplitude obtained from the respective test to the one obtained with the aluminum foil ($|R|$=1). We compared the reflection coefficients estimated by the radar measurements with the theoretical values, at different air-filled fracture apertures and at two significant frequencies, as predicted by the thin layer theory. The two selected frequencies correspond to the one with the highest energy in the spectra of the reflected signals (1600 MHz), and to the nominal frequency of the antenna (2000 MHz). For the marble and the air, respectively, we set a relative permittivity of 9.5 and 1 and a conductivity σ of 14 x10^{-4} S/m and 1x10^{-6} S/m (Vaccaneo *et al.*, 2004). For each frequency and material we calculated the wavelength λ, the attenuation coefficient α, the propagation factor β and the electromagnetic impedance Z. The results are reported in Table 1.
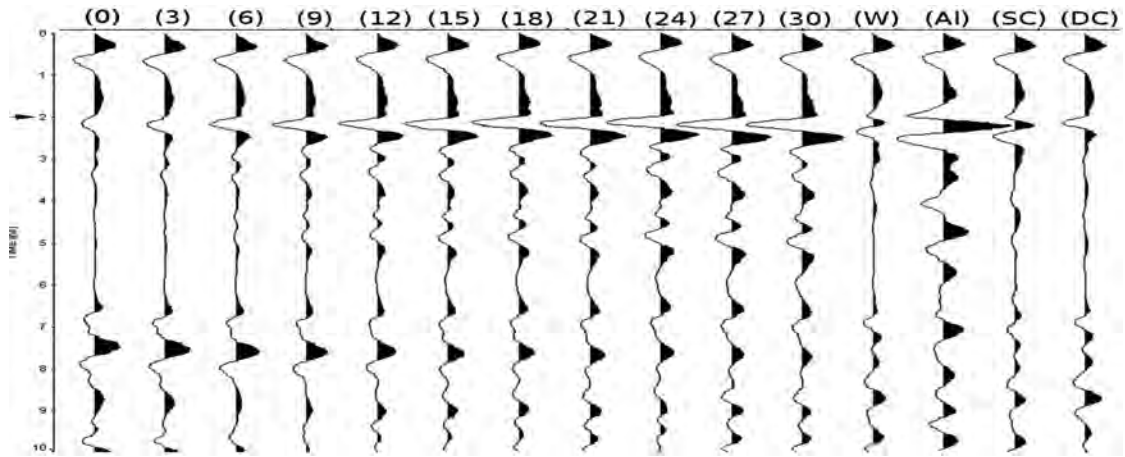
Fig. 7 - Comparison of the traces at Y=10 cm (central profile, Y direction, Ex) obtained with different apertures and fillings. The numbers from 0 to 30 identify the aperture in mm of the joint filled with air. The letters identify the filling materials: water (W), aluminum (Al), saturated cuttings (SC) and dry cuttings (DC,) respectively. The arrow on the left indicates the joint position.

It is evident that neither the marble nor the air have a significant attenuation factor and that they can be, therefore, assumed as lossless materials. According to this evidence, we applied the simplified formula for thin layer reflection usable when the thin layer is in between the same material:

$$\Gamma = \frac{R_{ma}\left(1 - e^{-i\frac{4\pi d}{\lambda_a}}\right)}{1 - R_{ma}{}^2 e^{-i\frac{4\pi d}{\lambda_a}}} \qquad (1)$$

Where:

Γ is the thin layer reflection coefficient;

d is the fracture aperture;

λ_a is the wavelength in the filling material (air);

R_{ma} is the reflection coefficient between marble and air when the air is a semi-infinite space

Table 1 - Electromagnetic parameters of the marble and the air.

	σ [S/m]	ε_r [-]	f [GHz]	α [1/m]	β [1/m]	λ [m]	V [m/ns]	Z [Ω]
marble	14×10^{-4}	9.5	1.6	0.086	103.3	0.06	0.097	$122.3 + i\,0.05$
			2.0	0.086	129.1	0.049	0.097	$122.3 + i\,0.04$
air	1×10^{-6}	1	1.6	1.9×10^{-4}	33.5	0.19	0.3	$377 + i\,2.1\times10^{-3}$
			2.0	1.9×10^{-4}	41.9	0.15	0.3	$377 + i\,1.7\times10^{-3}$

Table 2 - Reflection coefficients for the marble-air contrast estimated with the semi-infinite reflector formulation (R_{ma}) and with the thin reflector hypothesis (Γ) for different apertures d (2 mm, 9 mm, 18 mm and 27 mm) and frequencies f (1600 and 2000 MHz).

	f [GHz]	R_{ma} [-]	Γ[-]			
			d=2mm	d=2mm	d=18mm	d=27mm
marble	1.6	0.5-i1.5x10-4	0.010-i0.09	0.18-i0.34	0.47-i0.4	0.67-i0.31
/air	2.0	0.5-i1.2x10-4	0.016-i0.11	0.25-i0.38	0.58-i0.36	0.75-i0.21

and its value is given by:

$$R_{ma} = \frac{\sqrt{\varepsilon_m} - \sqrt{\varepsilon_a}}{\sqrt{\varepsilon_m} + \sqrt{\varepsilon_a}}$$

being ε_m the relative permittivity of marble and ε_a the relative permittivity of air.
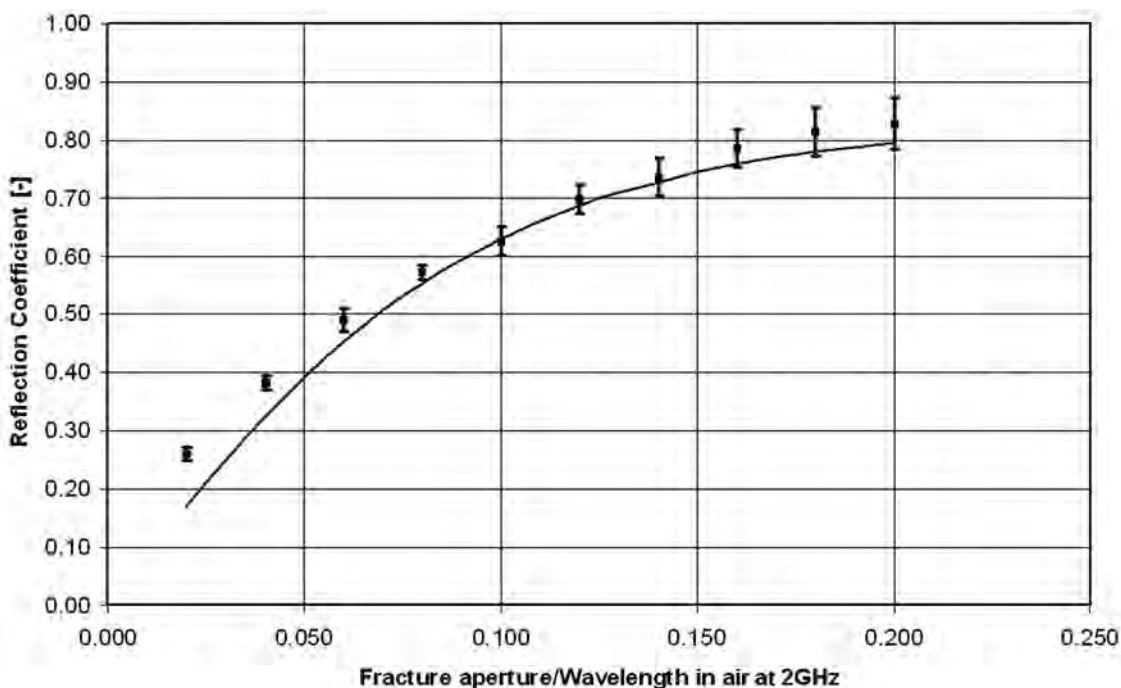

Fig. 8 - Comparison between the reflection coefficients Γ estimated from the thin layer reflector theory (black line) and the reflection coefficients estimated by radar measurements (black dots) with 3 times the standard deviations (black bar).

A more detailed analysis of the thin layer theory is reported in Appendix A.

Applying Eq. (1) to four fracture apertures of our experiment, we obtained the values shown in Table 2.

In Fig. 8, we plotted, versus each aperture, the mean and the 3 times standard deviation of the experimental values of Γ estimated by GPR measurements and the theoretical one obtained by Eq. (1) at 2 GHz. An acceptable fit is not achieved until the fracture has an aperture of 12 mm, which is about 1/12 of the wavelength in air. The best fit is obtained at 1/10 of the wavelength, for a higher aperture the fitting began to worsen even if the theoretical values feall within the experimental ±3 standard deviation range.

From the results of our experiment, we could guess a method able to provide information, in field conditions, on the fracture apertures with GPR near-zero offset reflection acquisition. A reference value for the GPR amplitude impinging the fracture must be estimated: this information could be provided by the reflection amplitude of a perfect reflector localized at the same depth of the fracture. This reference amplitude can be estimated by interpolating the reflection amplitudes obtained performing GPR measurements over sound blocks with different thicknesses and with an aluminium plate on the opposite side of the surveying plane. The ratio between the reflection amplitude due to the fracture and the one due to the perfect reflector is the thin layer reflection coefficient Γ. If the thin layer reflection coefficient Γ and the electromagnetic properties of the filling are known, Eq. (1) allows us to calculate the fracture aperture. This estimation would, however, be valid only if the fracture is roughly parallel to the acquisition plane and is the first discontinuity met by the GPR pulse.

4. Conclusions

Our experiments clearly indicate that the GPR with at 2 GHz antenna is a suitable tool to identify and locate fractures as thin as 1 mm in the "Bigio di Frabosa" marble, with all the expected filling materials. According to our experiments fracture apertures from 1/10 to 1/5 of the wavelength could be estimated by the thin-layer, reflection coefficient analysis, providing the fracture is parallel to the survey plane. We observed that the best fit between the theoretical and experimental reflection coefficients was obtained with the nominal frequency of the antenna (2 GHz). In this case, this frequency can also be considered as the upper limit of the frequency band of the reflected signals.

However, to estimate the actual value of the fracture apertures in the field is probably not an easy task, the knowledge of the filling material and some tests with a perfect reflector are needed.

Appendix A

Let us suppose to have a plane wave of amplitude E_0 and frequency f impinging almost vertically on a horizontal interface separating a medium 1 from a thin layer 2 of thickness d, overlaying a medium 3. In Fig. A1, the geometry and the physical parameters needed are sketched.

The near zero offset reflection and transmission coefficients are:

$$R_{i,i+1} = \frac{Z_{i+1} - Z_i}{Z_{i+1} + Z_i} \quad \text{and} \quad T_{i,i+1} = \frac{2Z_{i+1}}{Z_{i+1} + Z_i} \tag{A1}$$

being:

$$Z = \sqrt{\frac{i\omega\mu}{\sigma + i\omega\varepsilon}} \quad \text{or} \quad Z = \sqrt{\frac{\mu}{\varepsilon} \frac{1}{\left(\frac{\sigma}{i\omega\varepsilon} + 1\right)}} \tag{A2}$$

where σ is the conductivity, ε the electrical permittivity, μ the magnetic permeability, ω the angular frequency and Z the intrinsic impedance of the material.

Moreover, Maxwell's attenuation and propagation factors, α and β, have to be considered:

$$\alpha = \omega \sqrt{\frac{\mu\varepsilon}{2}\left[\sqrt{1 + \left(\frac{\sigma}{\omega\varepsilon}\right)^2} - 1\right]} \tag{A3}$$
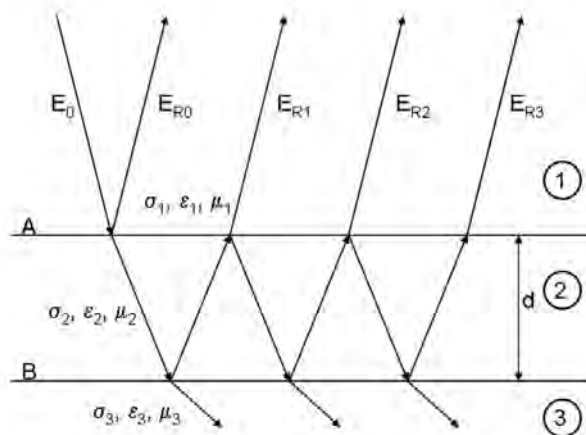

Fig. A1 - Scheme of multiple reflection within a thin layer with geometrical and physical parameters.

$$\beta = \omega \sqrt{\frac{\mu\varepsilon}{2}\left[\sqrt{1+\left(\frac{\sigma}{\omega\varepsilon}\right)^2}\right]+1} \qquad\qquad (A4)$$

Then, the reflected wave from interface A will be given by the interferences among E_{R0}, E_{R1}, E_{R2}, E_{R3}, E_{R4} and so on. If the thin layer has a constant thickness, it is easy to show that the phase delay and amplitude attenuation of the nth multiple reflected wave from interface B, with respect to E_{R0}, can be written as:

$$\varphi_n = 2nk_2 \qquad d = 2n\phi_2 \qquad\qquad (A5)$$

being $k_i = \alpha + \beta$ the complex wave number in medium 2 and $\phi = k_d$.

It is then be possible to write each single contribution of each multiple reflection to the reflection coefficient at the interface A taking into account for the phase delay and attenuation due to each multiple path as:

$$E_{R0} = E_0 R_{12}$$
$$E_{R1} = E_0 T_{12} R_{23} T_{21} e^{-2\cdot1\cdot\phi_2}$$
$$E_{R2} = E_0 T_{12} R_{23} R_{21} R_{23} T_{21} e^{-2\cdot2\cdot\phi_2}$$
$$E_{R3} = E_0 T_{12} R_{23} R_{21} R_{23} R_{21} R_{23} T_{21} e^{-2\cdot3\cdot\phi_2}.$$

Summing up the above expressions, isolating the first reflection and collecting a suitable factor, one obtains the general formula for m multiples:

$$E_R = E_0 R_{12} + E_0 R_{23} T_{12} T_{21} e^{-2\phi_2}\left\{\sum_{n=1}^{m}\left[\left(R_{23}R_{21}\right)e^{-2\phi_2}\right]^{(n-1)}\right\}. \qquad\qquad (A6)$$

The same equation can be found, written in a different manner, in Hollender and Tillard (1998).

Eq. (A6) can be written in a simpler, approximate form. In fact, the sum in the brackets is of the kind:

$$\sum_{i=0}^{m} x^i$$

that, providing $x^2 < 1$, can be expanded as $1/(1-x)$. Eq. (A6) can then be rewritten as:

$$E_R = E_0 R_{12} + \frac{E_0 R_{23} T_{12} T_{21} e^{-2\phi_2}}{1-\left(R_{23}R_{21}\right)e^{-2\phi_2}}$$

so that:

$$E_R = \frac{E_0 R_{12} - E_0 R_{23} R_{12} R_{21} e^{-2\phi_2} + E_0 R_{23} T_{12} T_{21} e^{-2\phi_2}}{1-\left(R_{23}R_{21}\right)e^{-2\phi_2}}$$

or also:

$$E_R = \frac{E_0 R_{12} + E_0 R_{23} e^{-2\phi_2}\left(T_{12}T_{21} - R_{12}R_{21}\right)}{1-\left(R_{23}R_{21}\right)e^{-2\phi_2}}$$

But E_R / E_0 is the reflection coefficient Γ and, given Eq. (A1), it is clear that $R_{12} = -R_{21}$ and $T_{12}T_{21} + R_{12}{}^2 = 1$. Then:

$$\Gamma = \frac{R_{12} + R_{23}e^{-2\phi_2}}{1 + R_{12}R_{23}e^{-2\phi_2}} \tag{A7}$$

If the lamina 2 is between the same material 1 then $R_{23} = - R_{12}$ and Eq. (A7) becomes:

$$\Gamma = \frac{R_{12}\left(1 - e^{-2\phi_2}\right)}{1 - R_{12}{}^2 e^{-2\phi_2}}. \tag{A8}$$

If , the complex wavenumber is defined as $k_2 = \beta_2 - i\alpha_2$ (Grégoire and Hollender, 2004) then Eqs. (A7) and (A8) respectively become:

$$\Gamma = \frac{R_{12} + R_{23}e^{-i2\phi_2}}{1 + R_{12}R_{23}e^{-i2\phi_2}}$$

and

$$\Gamma = \frac{R_{12}\left(1 - e^{-i2\phi_2}\right)}{1 - R_{12}{}^2 e^{-i2\phi_2}}.$$

that are the same equations that can be found in Grégoire and Hollender (2004).
Let's now suppose that:

$$\frac{\sigma_2}{\omega\varepsilon_2} \ll 1.$$

If this inequality holds, the dissipative phenomena are negligible (α_2=0) and the reflection and transmission coefficients could be written, looking at Eq. (A2) and considering $\left\{\mu_i = \mu_0,\ \left(\forall i\right)\right\}$, as:

$$R_{i,i+1} = \frac{\sqrt{\varepsilon_i} - \sqrt{\varepsilon_{i+1}}}{\sqrt{\varepsilon_{i+1}} + \sqrt{\varepsilon_i}} \quad \text{and} \quad T_{i,i+1} = \frac{2\sqrt{\varepsilon_i}}{\sqrt{\varepsilon_{i+1}} + \sqrt{\varepsilon_i}}. \tag{A9}$$

Moreover, remembering that the wavelength $\lambda = \dfrac{2\pi}{\beta}$, Eq. (A5) can be rewritten as:

$$\varphi_n = i2n\frac{2\pi}{\lambda_2}d$$

so that Eq. (A7) becomes:

$$\Gamma = \frac{R_{12} + R_{23}e^{-i\frac{4\pi d}{\lambda_2}}}{1 + R_{12}R_{23}e^{-i\frac{4\pi d}{\lambda_2}}} \tag{A10}$$

and Eq. (A8) becomes:

$$\Gamma = \frac{R_{12}\left(1 - e^{-i\frac{4\pi d}{\lambda_2}}\right)}{1 - R_{12}^{\ 2}e^{-i\frac{4\pi d}{\lambda_2}}}. \tag{A11}$$

That is the usual expression that can be found, for example, in Annan *et al.* (1988).

In Fig. A2, the reflection coefficient of a thin layer of clayey material within the marble is shown. Both plots from Eqs. (A8) and (A11) are presented and, for example, not to take for the dissipation into account, can lead to an overestimation of about 5% of the reflection coefficient when $d = \lambda/4$.
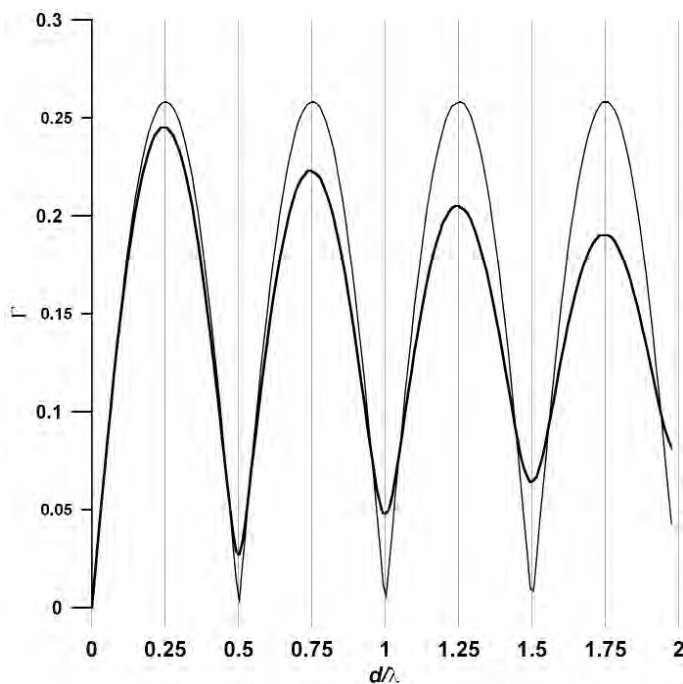

Fig. A2 - Absolute value of the thin layer reflection coefficient of a lamina having $\varepsilon = 16$, $\sigma = 0.1$ within a material having $\varepsilon = 9.5$, $\sigma = 0.002$ at $f = 1600$ MHz. The half-space reflection coefficient has an absolute value of 0.13. The thick black line represents Eq. (A8), the thin black line represents Eq. (A11).

REFERENCES

Al-Qadi I.L. and Lahouar S.; 2005: *Measuring layer thicknesses with GPR - Theory to practice*. Construction and Building Materials, **19**, 763-772.

Annan A.P., Davis J.L. and Gendzwill D.; 1988: *Radar sounding in potash mines, Saskatchewan, Canada*. Geophysics, **53**, 1556-1564.

Apel D.B. and Dezelic V.; 2005: *Evaluation of high frequency ground-penetrating radar (GPR) in mapping strata of dolomite and limestone rocks for ripping technique*. International Journal of mining, reclamation and environment, **19**, 260-275.

Dezelic V.; 2004: *Applications of ground penetrating radar (GPR) in mapping mine roof*. M. Sc. Thesis in mining engineering, University of Missouri-Rolla.

Ferrero A.M., Godio A., Sambuelli L. and Voyat I.H.; 2007: *Geophysical and geomechanical investigations applied to the rock mass characterisation for distinct element modelling*. Rock Mechanics and Rock Engineering, **40**, 603-622.

Grandjean G. and Gourry J.C.; 1996: *GPR data processing for 3D fracture mapping in a marble quarry (Thassos, Greece)*. Journal of Applied Geophysics, **36**, 19-30.

Grasmueck M.; 1996: *3-D ground-penetrating radar applied to fracture imaging in gneiss*. Geophysics, **61**, 1050-1064.

Grégoire C., Halleux L. and Vervoort A.; 2003: *Application of ground penetrating radar in a mining environment*. In: University of Mining and Geology "St. Ivan Rilski", Annual, vol. 46, part II, Mining and Mineral Processing, Sofia, pp. 179-183.

Grégoire C. and Hollender F.; 2004: *Discontinuity characterization by the inversion of the spectral content of ground-penetrating radar (GPR) reflections—Application of the Jonscher model*. Geophysics, **69**, 1414-1424.

Guha S.; 2004: *Ground penetrating radar response to thin layers: examples from Waites Island, South Carolina*. M. Sc. Thesis. Department of geology, University of South Florida.

Hollender F. and Tillard S.; 1998: *Modeling ground penetrating radar wave propagation and reflection with the Jonscher parametrization*. Geophysics, **63**, 1933-1942.

Koh G.; 1997: *Complex dielectric constant of ice at 1.8 GHz*. Cold region science and technology, **25**, 119-121.

Lahouar S. and Al-Qadi I.L.; 2008: *Automatic detection of multiple pavement layers from GPR data*. NDT&E International, **41**, 69-81.

Myeong-Jong Y., Jung-Ho K. and Seong-Jun C.; 2004: *Integrated application of borehole radar reflection and resistivity tomography to delineate fractures in granite quarry mine*. In: Tenth International Conference on Ground Penetrating Radar, Delft., BHR2, pp. 213-216.

O'Neill K.; 2000: *Radar sensing of thin surface layers and near-surface buried objects*. IEEE Transactions on Geoscience and Remote Sensing, **38**, 480-495.

Porsani J.L., Sauck W.A. and Júnior A.O.S.; 2006: *GPR for mapping fractures and as a guide for the extraction of ornamental granite from a quarry: a case study from southern Brazil*. Journal of Applied Geophysics, **58**, 177-187.

Riek L., Crane R.K. and O'Neill K.; 1990: *A signal-processing algorithm for the extraction of thin freshwater-ice thickness from short pulse radar data*. IEEE Transactions on Geoscience and Remote Sensing, **28**, 137-145.

Talley J., Baker G.S., Becker M.W. and Beyrle N.; 2005: *Four dimensional mapping of tracer channelization in sub-horizontal bedrock fractures using surface ground penetrating radar*. Geophysical Research Letters, **32**, L04401, 1-4.

Tsoflias G.P., Gestel J.P.V., Stoffa P.L., Blankenship D.D. and Sen M.; 2004: *Vertical fracture detection by exploiting the polarization properties of ground-penetrating radar signals*. Geophysics, **69**, 803-810.

Vaccaneo D., Sambuelli L., Marini P., Tascone R. and Orta R.; 2004: *Measurement system of complex permittivity of ornamental rocks in L frequency band*. IEEE transactions on geoscience and remote sensing, **42**, 2490-2498.

Yamamoto M., Ikeya K., Inagaki M. and Koyama T.; 2004: *A vector diagram to determine anomaly conditions in a thin layer*. In: Proceedings of Tenth International Conference on GPR, Delft, The Nederlands, CPE7, pp. 647-650.

Corresponding author: Luigi Sambuelli
                          DITAG, Politecnico di Torino
                          Corso Duca degli Abruzzi 24, 10129 Torino, Italy
                          phone: +39 01 10907665; fax: +39 01 10907699; e-mail: luigi.sambuelli@polito.it